ACS Sustainable Chemistry & Engineering

Letter

pubs.acs.org/journal/ascecg

Synthetic Design of Gold Nanoparticles on Anatase TiO_2 {001} for Enhanced Visible Light Harvesting

Junqing Yan, Guangjun Wu, Weili Dai, Naijia Guan, and Landong Li*

Key Laboratory of Advanced Energy Materials Chemistry (Ministry of Education), College of Chemistry, Nankai University, Tianjin 300071, P.R. China

Supporting Information

ABSTRACT: A simple and green photodeposition route is developed for the selective deposition of Au nanoparticles on anatase TiO_2 {001} facets to prepare a Au−TiO_2 localized surface plasmon resonance photocatalyst system. The surface-capping agents on Au nanoparticles can be completely removed during the photodeposition process, and the close contact between the Au and TiO_2 support in the as-prepared Au−TiO_2 system is guaranteed, as confirmed by thermogravimetric and X-ray photoelectron spectroscopy analyses. Accordingly, the separation of photogenerated electron−hole pairs via localized surface plasmon resonance is greatly enhanced, and promoted activity of Au−TiO_2 in both photocatalytic hydrogen evolution and methylene blue decomposition could be obtained under visible light irradiation.

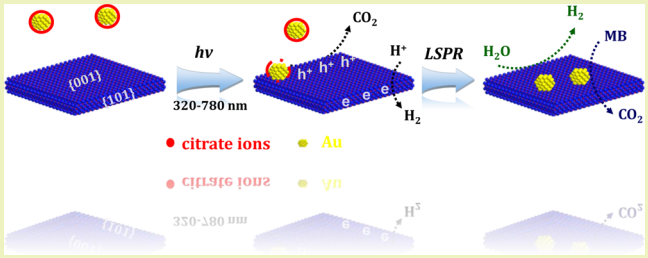

KEYWORDS: *Selective deposition, Au nanoparticles, Green route, LSPR*

INTRODUCTION

Semiconductor photocatalysis has attracted extensive attention due to its potential application in environment remediation and solar energy conversion, and current researches focus on photocatalysis under visible light with the aim to make better use of solar light.[1−4] Recently, localized surface plasmon resonance (LSPR) photosensization has been recognized as a promising strategy to achieve visible light harvesting with metal Au or Ag nanostructures on semiconductor TiO_2 as the most familiar examples.[5−11] The electrons in metals might be excited by the LSPR with visible light absorption and subsequently transfer to the conduction band of the attached semiconductors. The electrons transferred to the surface of semiconductor and the holes remaining on the surface of the metals can act as redox centers to initiate photocatalytic reactions.[5,10] Extensive research is focused on controlling the physical properties of plasmonic metals, e.g. size and shape, and their impacts on the LSPR intensity and corresponding visible light-driven activity.[12−17] In contrast, relatively less research is involved in the effects of support materials and preparation strategies on LSPR intensity, which are also very important issues in LSPR photocatalysis.[18−20]

TiO_2 is a favorable support for plasmonic metals due to its high electron injection ability. The exposed facet of the TiO_2 crystal is very important, and the photocatalytic activity of different facets has been sufficiently debated in recent years.[21−25] For anatase TiO_2, it is well acknowledged that its high-energy {001} facets prefer to provide the oxidation sites, while the low-energy {101} facets prefer to provide the reduction sites.[26−28] Thus, the driving of photogenerated electrons and holes to different facets under irradiation offers great opportunity for the selective photodeposition of co-catalysts on designated facets of pristine semiconductors, e.g., $BiVO_3$ {010}/{110} and WO_3 {040}.[29,30]

Herein, we report a new and green synthesis strategy to Au on TiO_2 {001} facets via selective photodeposition. The close contact between Au and TiO_2 {001} facets is ensured by the photodeposition route, which results in enhanced LSPR intensity and accordingly greatly promotes photocatalytic activity under visible light irradiation. We further demonstrate that other parameters, e.g., the percentage of {001} facets in the TiO_2 support and size of the Au nanoparticles, can also influence the LSPR-induced photocatalytic activity under visible light irradiation. All of these parameters, i.e., Au−TiO_2 interaction, TiO_2 facet, and Au size, are mutually tolerant to each other, and therefore, the rational design of the robust composite structure for visible light harvesting via LSPR is possible.

RESULTS AND DISCUSSION

Anatase TiO_2 nanosheets with {001} as the dominating exposed facet were prepared via a hydrothermal method,[31−33] and the percentage of exposed {001} facet can be adjusted by changing the HF/TiO_2 ratio, as calculated and summarized in Table 1.[34,35] The anatase TiO_2 nanosheets appear as light gray, which results in additional absorbance in the visible light region (Figure S1, Supporting Information). The colloidal Au nanoparticles were prepared based on the sodium citrate

Received: May 23, 2014
Revised: July 15, 2014
Published: July 22, 2014

Table 1. Physicochemical Properties of Anatase TiO_2 Nanosheets

sample	HF/TiO_2[a]	crystallite size (length × width × thickness)	percentage[b] {001} (%)	percentage[c] {001} (%)	S_{BET} (m^2/g)	color
TiO_2-1/1	1/1	30 nm × 30 nm × 7 nm	68	58	85	light gray
TiO_2-3/2	3/2	40 nm × 40 nm × 6 nm	77	66	78	light gray
TiO_2-2/1	2/1	45 nm × 45 nm × 6 nm	80	73	80	light gray
TiO_2-5/2	5/2	50 nm × 50 nm × 5 nm	83	77	75	light gray

[a]Mole ratio. [b]Calculated based on XRD patterns. [c]Calculated based on Raman spectra.

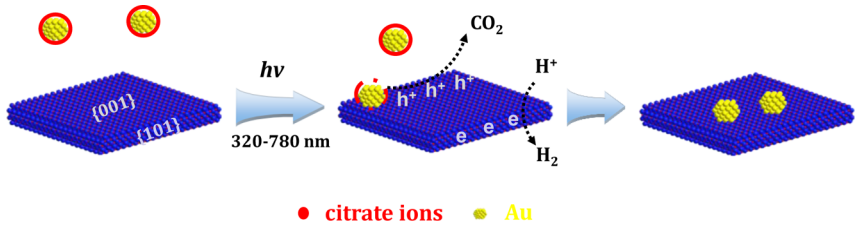

Figure 1. Synthetic strategy to Au nanoparticles on TiO_2 {001}.

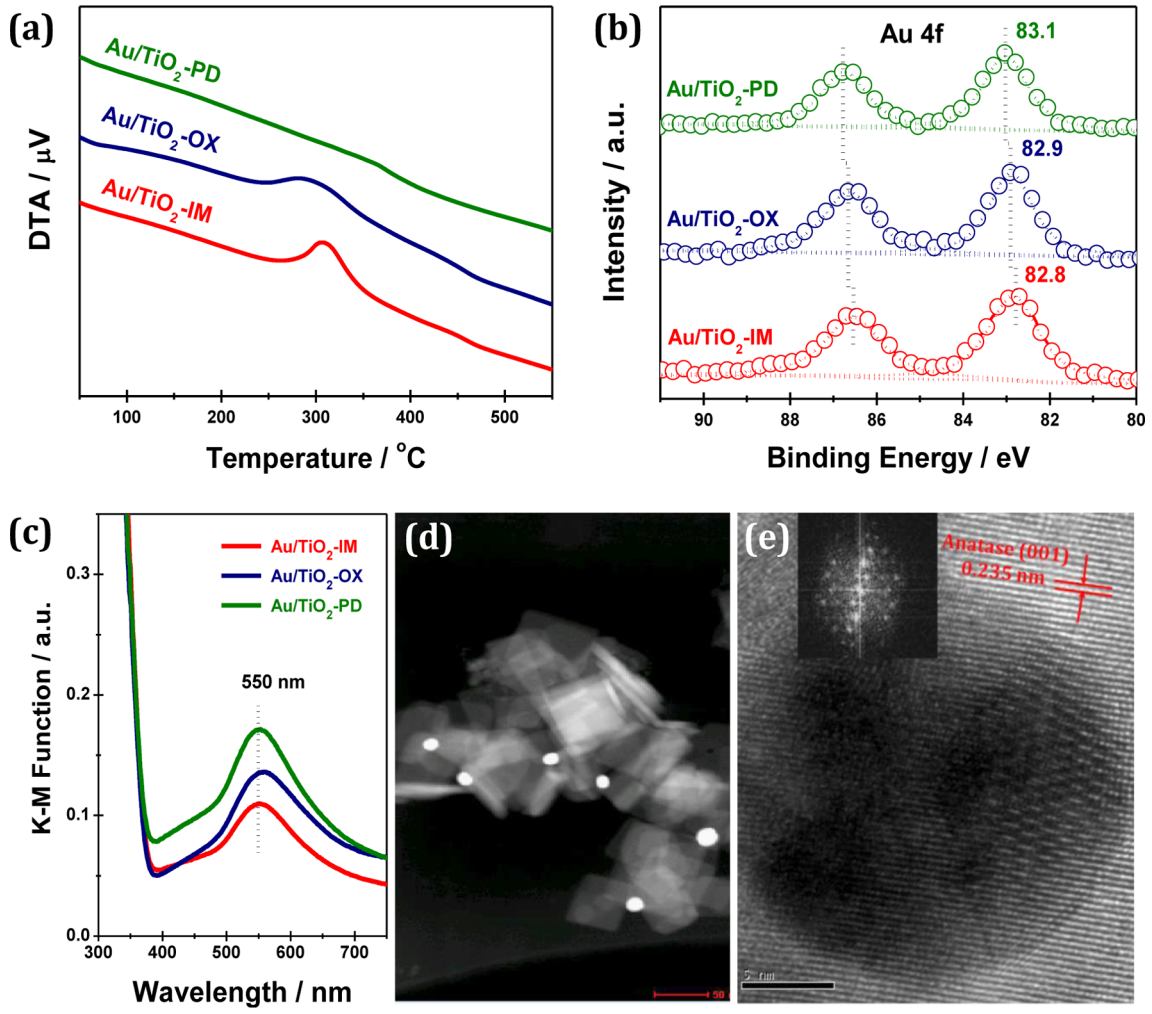

Figure 2. (a) DTA curves of Au−TiO_2-2/1 prepared by different methods. (b) Au 4f XPS of Au−TiO_2-2/1 samples. (c) UV−vis spectra of Au−TiO_2-2/1 samples. (d) HAADF-STEM image of Au−TiO_2-2/1−PD. (e) HRTEM image of Au−TiO_2-2/1−PD with FFT analysis of the Au nanoparticle (inset).

reduction method as developed by Frens.[36] In this process, citrate ions not only act as the reducing agent for colloidal Au but also act as the surface-capping agent to stabilize the colloidal Au. The as-prepared colloidal Au nanoparticles appear as ruby red, and the UV−vis spectrum shows a distinct peak centered at about 530 nm as a result of Au plasmon resonance (Figure S2, Supporting Information). The TEM analysis confirms that colloidal Au nanoparticles are obtained as expected, and the average size of colloidal Au nanoparticles is estimated to be ∼9 nm (Figure S3, Supporting Information).

dx.doi.org/10.1021/sc500331k | ACS Sustainable Chem. Eng. 2014, 2, 1940−1946

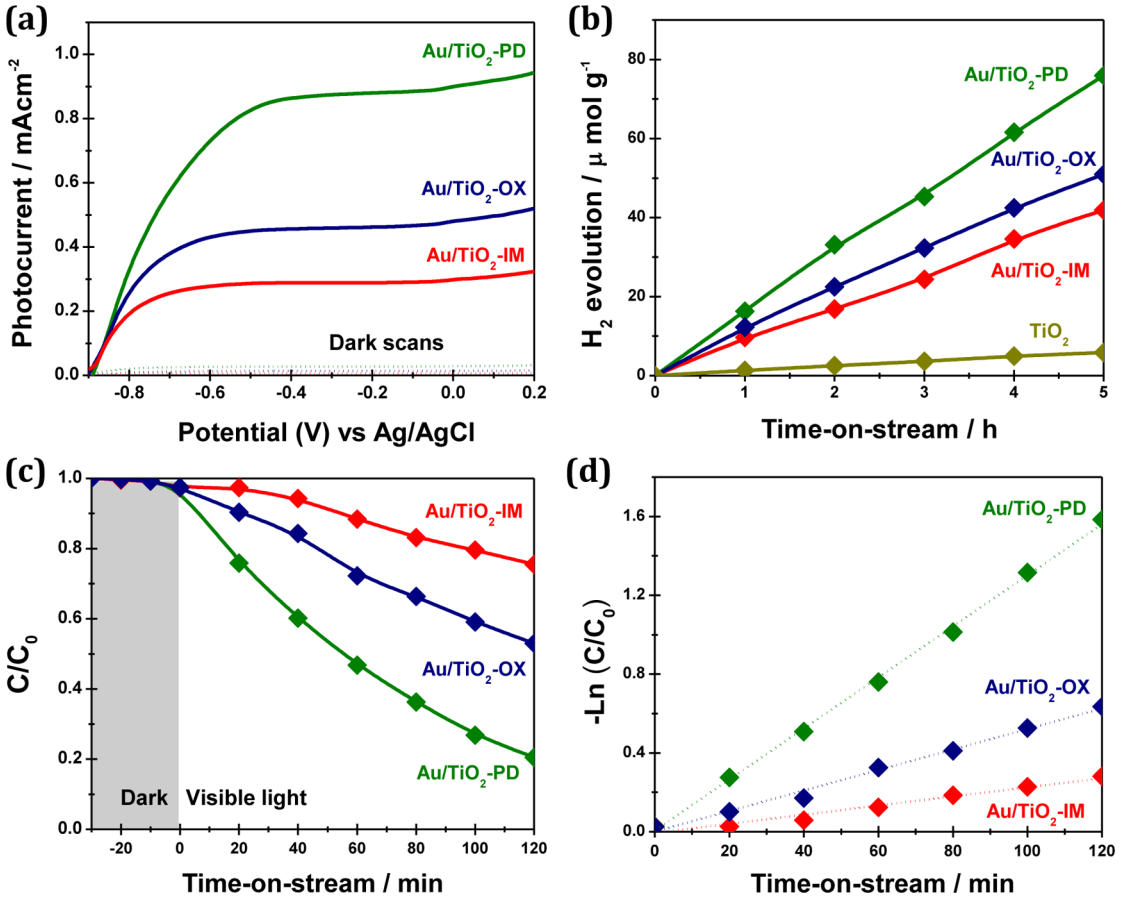

Figure 3. (a) Photocurrent response of Au−TiO_2-2/1 samples prepared by different methods in 1.0 M KOH with a scan rate of 50 mV/s under visible illumination (λ > 400 nm). (b) Photocatalytic hydrogen evolution over Au−TiO_2-2/1 samples under visible light (λ > 400 nm); 1% Pt was in situ loaded as co-catalyst. (c,d) Photocatalytic decomposition of MB over Au−TiO_2-2/1 samples under visible light (λ > 400 nm).

Au nanoparticles were selectively deposited on anatase TiO_2 {001} facets via a newly developed simple and green route, where no toxic reagents were employed and no post-treatments were required. The cartoon of synthetic strategy is described in Figure 1, and the essence of the strategy is a photocatalytic redox reaction. Under UV−visible irradiation, the photogenerated holes and electrons in TiO_2 will migrate to {001} and {101} facets, respectively, according to the preferential flow of photogenerated carriers to the specific facets with different energy.[23] Moreover, electrons can be excited due to the SPR effects of Au and accumulate on the Au surface. The electrostatic attraction will drive the Au nanoparticles to the positively charged anatase {001} facets, where the citrate ions on the surface of the Au will be oxidized to CO_2 by the photogenerated holes. Meanwhile, the H^+ in the solution would be reduced to H_2 by photogenerated electrons on anatase TiO_2 {101} facets as the other half of the reaction.

The photodeposition process is monitored by temporal analysis of the filtrated Au colloid during photodeposition. The color of the Au colloid gradually turned from the original ruby red to light red and finally to colorless with time-on-stream of photodeposition (Figure S6, inset, Supporting Information). The UV−vis spectra indicated gradual decreases in the intensity of peak centered at about 530 nm corresponding to Au plasmon resonance, confirming the disappearance of Au in the liquid phase (Figure S6, Supporting Information). These results clearly reveal the loading of Au on the TiO_2 support via the photodeposition process. The efficiency of photodeposition can be higher than 99% providing sufficient time is employed for photodeposition (6 h in the case of Au−TiO_2-5/2). Accompanied by the photodeposition of Au, H_2 evolution can be observed as a result of photocatalytic reduction of water. The rate of H_2 evolution is dependent on the anatase TiO_2 supports employed, and higher H_2 evolution rates are obtained with higher percentages of {001} facets exposed (Figure S7, Supporting Information). This is explained as the result of better separation of photogenerated electron−hole pairs with a higher percentage of {001} facets exposed.

For a better understanding of the advantages of our photodeposition method and their impacts on LSPR photocatalysis, several characterization techniques are further employed. Figure 2a shows the DTA curves of the Au−TiO_2 samples prepared by different methods. For Au−TiO_2−IM (prepared via incipient wetness impregnation), an obvious exothermic peak at 310 °C is observed originating from the oxidation of the organic species, i.e., citrate ions. For samples treated with $HClO_4$, i.e., Au−TiO_2−OX, the intensity of the exothermic peak greatly decreases and shifts to lower temperature due to the removal of most organic species during $HClO_4$ oxidation.[19] In contrast, no exothermic peak can be observed for Au−TiO_2−PD, indicating the complete removal of organic species during photodeposition. It is known that the existence of surface-capping agents will enlarge the distance between plasmonic metals, which leads to the attenuation in the LSPR intensity. Therefore, the surface-capping agents are removed for the LSPR photocatalyst system. Compared with

dx.doi.org/10.1021/sc500331k | ACS Sustainable Chem. Eng. 2014, 2, 1940−1946

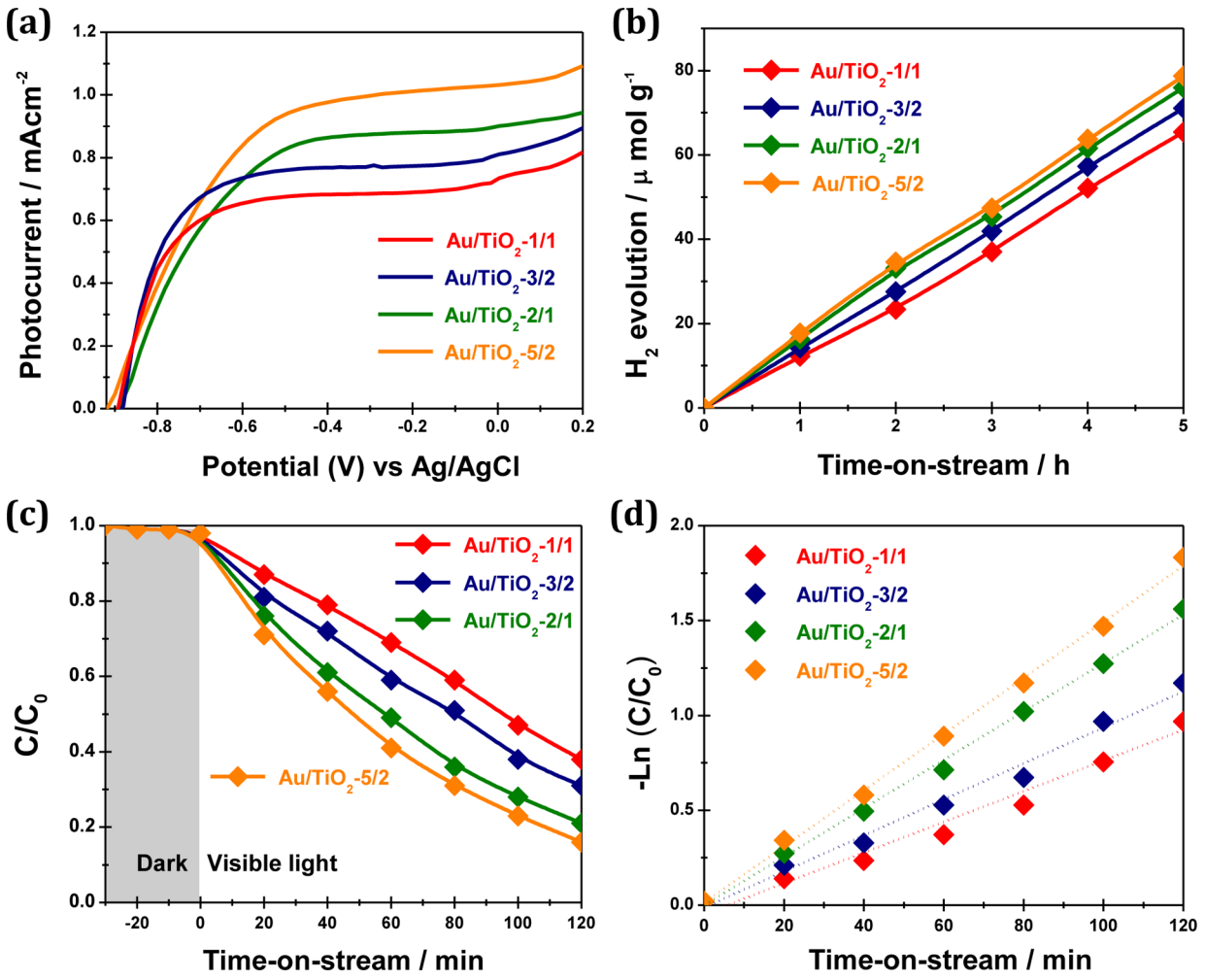

Figure 4. (a) Photocurrent response of Au−TiO_2−PD samples in 1.0 M KOH with a scan rate of 50 mV/s under visible illumination (λ > 400 nm). (b) Photocatalytic hydrogen evolution over Au−TiO_2−PD samples under visible light (λ > 400 nm); 1% Pt was in situ loaded as co-catalyst. (c,d) Photocatalytic decomposition of MB over Au−TiO_2−PD samples under visible light (λ > 400 nm).

other routes, the photodeposition route is a completely green one, and H_2/CO_2 is released as a harmless byproduct. Moreover, the absence of a calcination step is energy saving, and the aggregation of Au nanoparticles could be avoided. The Au−TiO_2 interaction is investigated by means of XPS. As shown in Figure 2b, binding energy values of 82.8 and 86.4 eV are observed for Au−TiO_2−IM, corresponding to Au $4f_{7/2}$ and $4f_{5/2}$, respectively.[37,38] The binding energy values are somewhat lower than those of the reference Au foil, i.e., 83.8 and 87.4 eV. Considering that binding energy values of 82.8 and 86.4 eV are also observed for Au nanoparticles (Figure S8, Supporting Information), the lower binding energy values are due to the interaction between the Au and TiO_2 support as well as the residual capping agent and corresponding changes in the microenvironments of Au nanoparticles. A small shift of about 0.1 eV in the binding energy values is observed after the removal of surface-capping agents by $HClO_4$ oxidation (Au−TiO_2−OX). While for Au−TiO_2−PD, an obvious shift of 0.3 eV compared with that of Au−TiO_2−IM can be observed, indicating the different chemical environments of Au and the Au−TiO_2 interactions. UV−vis spectra show SPR peaks centered at about 550 nm for all Au−TiO_2 samples (Figure 2c). The red-shift in the SPR peaks of Au−TiO_2 relative to the Au colloid precursor (about 530 nm, Figure S2, Supporting Information) are due to the overall increase in the refractive index.[9] Interestingly, it is clearly observed that Au−TiO_2−PD exhibits higher SPR intensity than Au−TiO_2−OX and Au−TiO_2−IM, which originated from the removal of surface-capping agents and the close contact between Au and TiO_2.

The structure and morphology of the as-prepared Au−TiO_2−PD sample are investigated by means of microscopy. The TEM (Figure S10, Supporting Information) and HAADF-STEM images (Figure 2d) reveal that Au nanoparticles are successfully loaded on the TiO_2 support through photodeposition, and no aggregation or growth of Au nanoparticles could be observed. The HRTEM image in Figure 2e further reveals that a well-crystallized Au nanoparticle is deposited on the anatase TiO_2 {001} facet with lattice spacing of 0.235 nm, similar to a previous report.[19] The close contact between Au and TiO_2 {001} can also be supported by the HRTEM image. In contrast, the loose contact between Au nanoparticles and TiO_2 is observed in the HRTEM image of Au−TiO_2−IM, and the unambiguous Au FFT pattern indicates the existence of surface-capping agents (Figure S11, Supporting Information), consistent with DTA analysis results.

The visible light harvesting properties of Au−TiO_2 samples are illustrated by means of photocurrent responses and photocatalytic evaluation. As shown in Figure 3a, almost no

dx.doi.org/10.1021/sc500331k | ACS Sustainable Chem. Eng. 2014, 2, 1940−1946

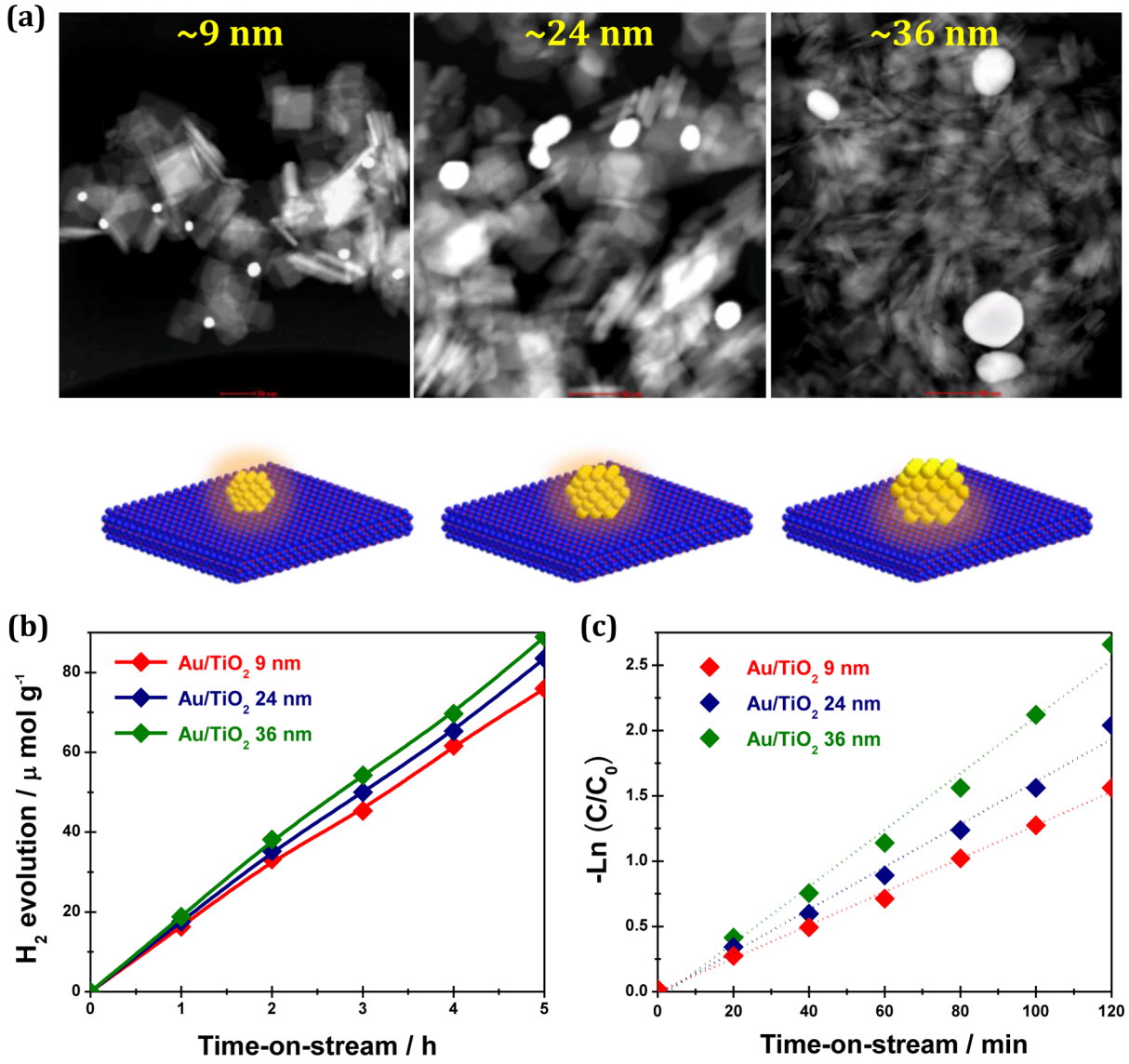

Figure 5. (a) HAADF-STEM images and structure models of Au−TiO_2-2/1−PD with different Au sizes. (b) Photocatalytic hydrogen evolution over Au−TiO_2-2/1−PD samples under visible light (λ > 400 nm); 1% Pt was in situ loaded as co-catalyst. (c) Photocatalytic decomposition of MB over Au−TiO_2-2/1−PD samples under visible light (λ > 400 nm).

photocurrent responses were observed for all Au−TiO_2 samples in the dark, while obvious current responses were discerned from −0.8 to 0.2 eV (versus Ag/AgCl) under visible light illumination (λ > 400 nm). Au−TiO_2−PD shows a stable photocurrent density of about 0.9 mA/cm^2, several times higher than that of Au−TiO_2−OX (about 0.4 mA/cm^2) or Au−TiO_2−IM (about 0.3 mA/cm^2) with similar Au loading. The enhanced photocurrent response is related to the selective deposition of Au on anatase {001} facets, removal of surface-capping agents on Au, and subsequent close contact between Au and TiO_2 (vide supra). On the basis of the results from photocurrent responses, it is rational to propose that Au−TiO_2−PD exhibits higher photocatalytic activity than Au−TiO_2−OX and Au−TiO_2−IM. This is clearly confirmed by their activity difference in both the photocatalytic reduction reaction, i.e., hydrogen evolution from water splitting (Figure 3b), and photocatalytic oxidation reaction, i.e., MB decomposition (Figure 3c,d), under visible light irradiation.

We further investigate the effects of the TiO_2 support on the visible light harvesting properties of Au−TiO_2 prepared by photodeposition. Here, anatase TiO_2 nanosheets with different percentages of {001} facets exposed (Table 1) are employed as supports of Au nanoparticles. It is observed that a higher photocurrent is obtained with Au−TiO_2−PD with a higher percentage of {001} facets exposed (Figure 4a). Moreover, Au−TiO_2−PD with a higher percentage of {001} facets exposed exhibits higher photocatalytic activity in both hydrogen evolution from water splitting (Figure 4b) and MB decomposition (Figure 4c,d). This is due to the enhanced separation of photogenerated electron−hole pairs separation with exposed {001} facets.[35]

On the other hand, the LSPR intensity in the plasmonic photocatalyst system has been reported to be very much dependent on the size of the plasmonic metals.[12,13] Herein, we employed Au nanoparticles with different sizes (~9, ~24, and ~36 nm) for photodeposition on TiO_2. As expected, Au nanoparticles can be selectively deposited on anatase TiO_2 {001} facets with perfect efficiency (>99%, Figure 5a). Increase in the size of the Au nanoparticles has a positive effect on visible light harvesting ability, and Au−TiO_2−PD with a larger

dx.doi.org/10.1021/sc500331k | ACS Sustainable Chem. Eng. 2014, 2, 1940−1946

Au size exhibits distincly higher activity than that of a smaller Au size in both photocatalytic hydrogen production from water splitting (Figure 5b) and photocatalytic MB decomposition (Figure 5c). A direct comparison between our Au−TiO_2 catalysts with conventional ones is summarized in Table S1 of the Supporting Information.

Colloidal metal nanoparticles with surface-capping agents have been extensively employed for the preparation of supported metal nanocomposites for catalytic applications.[39−41] The removal of surface-capping agents, or so-called ligands, is a crucial issue considering that the existence of surface-capping agents may show great negative impacts on catalytic performances. Compared with other routes, e.g., thermal or oxidative treatments and solvent exaction,[42−44] the newly developed photodeposition route appears to be simpler, greener, and more selective to specific facets although it is limited to the use of semiconductor as the support. Because the structure of colloidal metals can be well preserved during photodeposition, the photodeposition route provides an elegant solution for the investigation of the effects of metal size and shape on the (photo)-catalytic performances. In the specific example of the Au−TiO_2 LSPR photocatalyst system, the photodeposition route can be applied in the loading of Au nanoparticles with different sizes onto anatase TiO_2 with different facets exposed. In this context, it presents a link between the plasmonic metal and semiconductor and allows us a better understanding of the LSPR effects.

In summary, we have successfully developed a simple and green strategy for the selective photodeposition of Au nanoparticles on anatase TiO_2 {001} facets, and a Au−TiO_2 LSPR photocatalyst system can be prepared. During photodeposition, the surface-capping agents on Au can be completely removed, and a close contact between the Au and anatase {001} facet is guaranteed. The close contact between the Au and anatase {001} facet leads to enhanced LSPR intensity and promotes the separation of photogenerated electron−hole pairs under visible light irradiation. Therefore, enhanced photocurrent response and photocatalytic activity can be obtained. For the as-prepared Au−TiO_2 LSPR photocatalyst system, different factors, i.e., plasmonic Au, semiconductor TiO_2 support, and their interactions, may influence the LPSR intensity simultaneous. However, these factors are mutually tolerant to each other, and therefore, it is possible to design robust composite structures for visible light harvesting via LSPR. The synthetic strategy developed in the present study can be extended to the deposition of colloidal metal nanostructures on semiconductor supports for various applications, and the well-defined structure of as-obtained product is particularly important for further structure−activity relationship studies.

■ ASSOCIATED CONTENT

Ⓢ Supporting Information

Experimental details and more characterization and catalytic results. This material is available free of charge via the Internet at http://pubs.acs.org.

■ AUTHOR INFORMATION

Corresponding Author

*E-mail: lild@nankai.edu.

Notes

The authors declare no competing financial interest.

■ ACKNOWLEDGMENTS

We thank Prof. Xueping Gao at Nankai University for his help on photocurrent measurements. This work is financially supported by the Collaborative Innovation Center of Chemical Science and Engineering (Tianjin) and the Ministry of Education of China (IRT-13R30, IRT-13022). Support from 111 Project (B12015) and Ph.D. Candidate Research Innovation Fund of Nankai University is also acknowledged.

■ REFERENCES

(1) Hoffmann, M. R.; Martin, S. T.; Choi, W.; Bahnemann, D. W. Environmental applications of semiconductor photocatalysis. *Chem. Rev.* **1995**, *95*, 69−96.

(2) Hernandez-Alonso, M. D.; Fresno, F.; Suarez, S.; Coronado, J. M. Development of alternative photocatalysts to TiO_2: Challenges and Opportunities. *Energy Environ. Sci.* **2009**, *2*, 1231−1257.

(3) Chen, C. C.; Ma, W. H.; Zhao, J. C. Semiconductor-mediated photodegradation of pollutants under visible-light irradiation. *Chem. Soc. Rev.* **2010**, *39*, 4206−4219.

(4) Tong, H.; Ouyang, S. X.; Bi, Y. P.; Umezawa, N.; Oshikiri, M.; Ye, J. H. Nano-photocatalytic materials: Possibilities and challenges. *Adv. Mater.* **2012**, *24*, 229−251.

(5) Tian, Y.; Tatsuma, T. Mechanisms and applications of plasmon-induced charge separation at TiO_2 films loaded with gold nanoparticles. *J. Am. Chem. Soc.* **2005**, *127*, 7632−7637.

(6) Awazu, K.; Fujimaki, M.; Rockstuhl, C.; Tominaga, J.; Murakami, H.; Ohki, Y.; Yoshida, N.; Watanabe, T. A plasmonic photocatalyst consisting of silver nanoparticles embedded in titanium dioxide. *J. Am. Chem. Soc.* **2008**, *130*, 1676−1680.

(7) Tada, H.; Kiyonaga, T.; Naya, S. Rational design and applications of highly efficient reaction systems photocatalyzed by noble metal nanoparticle-loaded titanium(IV) dioxide. *Chem. Soc. Rev.* **2009**, *38*, 1849−1858.

(8) Linic, S.; Christopher, P.; Ingram, D. B. Plasmonic-metal nanostructures for efficient conversion of solar to chemical energy. *Nat. Mater.* **2011**, *10*, 911−921.

(9) She, Z. W.; Liu, S. H.; Low, M.; Zhang, S. Y.; Liu, Z. L.; Mlayah, A.; Han, M. Y. Janus Au-TiO_2 photocatalysts with strong localization of plasmonic near-fields for efficient visible-light hydrogen generation. *Adv. Mater.* **2012**, *24*, 2310−2314.

(10) Yan, J.; Wu, G.; Guan, N.; Li, L. Synergetic promotion of photocatalytic activity of TiO_2 by gold deposition under UV-visible light irradiation. *Chem. Commun.* **2013**, *49*, 11767−11769.

(11) Hou, W.; Cronin, S. B. A review of surface plasmon resonance-enhanced photocatalysis. *Adv. Funct. Mater.* **2013**, *23*, 1612−1619.

(12) Liu, Z.; Hou, W.; Pavaskar, P.; Aykol, M.; Cronin, S. B. Plasmon resonant enhancement of photocatalytic water splitting under visible illumination. *Nano Lett.* **2011**, *11*, 1111−1116.

(13) Ingram, D. B.; Linic, S. Water splitting on composite plasmonic-metal/semiconductor photoelectrodes: evidence for selective plasmon-induced formation of charge carriers near the semiconductor surface. *J. Am. Chem. Soc.* **2011**, *133*, 5202−5205.

(14) Zhen, Z.; Huang, B.; Qin, X.; Zhang, X.; Dai, Y.; Whangbo, M.-H. Facile in situ synthesis of visible-light plasmonic photocatalysts M@TiO_2 (M = Au, Pt, Ag) and evaluation of their photocatalytic oxidation of benzene to phenol. *J. Mater. Chem.* **2011**, *21*, 9079−9087.

(15) Su, F.; Wand, T.; Lv, R.; Zhang, J.; Zhang, P.; Lu, J.; Gong, J. Dendritic Au/TiO_2 nanorod arrays for visible-light driven photoeletrochemical water splitting. *Nanoscale* **2013**, *5*, 9001−9009.

(16) DeSario, P. A.; Pieron, J. J.; DeVantier, D. E.; Brintlinger, T. H.; Stroud, R. M.; Rolison, D. R. Plasmonic enhancement of visible-light water splitting with Au−TiO_2 composite aerogels. *Nanoscale* **2013**, *5*, 8073−8083.

(17) Liu, W. L.; Lin, F. C.; Yang, Y. C.; Huang, C. H.; Gwo, S.; Huang, M. H.; Huang, J. S. The influence of shell thickness of Au@TiO_2 core−shell nanoparticles on the plasmonic enhancement effect in dye-sensitized solar cells. *Nanoscale* **2013**, *5*, 7953−7962.

(18) Zhu, S.; Liang, S.; Gu, Q.; Xie, L.; Wang, J.; Ding, Z.; Liu, P. Effect of Au supported TiO_2 with dominant exposed {001} facets on the visible-light photocatalytic activity. *Appl. Catal., B* **2012**, *119*−*120*, 146−155.
(19) Liu, L.; Ouyang, S.; Ye, J. Gold-nanorod-photosensitized titanium dioxide with wide-range visible-light harvesting based on localized surface plasmon resonance. *Angew. Chem., Int. Ed.* **2013**, *52*, 6689−6693.
(20) Long, J.; Chang, H.; Gu, Q.; Xu, J.; Fan, L.; Wang, S.; Zhou, Y.; Wei, W.; Huang, L.; Wang, X.; Liu, P.; Huang, W. Gold-plasmon enhanced solar-to-hydrogen conversion on the {001} facets of anatase TiO_2 nanosheets. *Energy Environ. Sci.* **2014**, *7*, 973−977.
(21) Liu, S.; Yu, J.; Jaroniec, M. Anatase TiO_2 with dominant high-energy {001} facets: Synthesis, Properties, and Applications. *Chem. Mater.* **2011**, *23*, 4085−4093.
(22) Yang, H. G.; Sun, C. H.; Qiao, S. Z.; Zou, j.; Liu, G.; Smith, S. C.; Cheng, H. M.; Lu, G. Q. Anatase TiO_2 single crystals with a large percentage of reactive facets. *Nature* **2008**, *453*, 638−641.
(23) Tachikawa, T.; Yamashita, S.; Majima, T. Evidence for crystal-face-dependent TiO_2 photocatalysis from single-molecule imaging and kinetic analysis. *J. Am. Chem. Soc.* **2011**, *133*, 7197−7204.
(24) Pan, J.; Liu, G.; Lu, G. Q.; Cheng, H. M. On the true photoreactivity order of {001}, {010}, and {101} facets of anatase TiO_2 crystals. *Angew. Chem., Int. Ed.* **2011**, *50*, 2133−2137.
(25) Gordon, T. R.; Cargnello, M.; Paik, T.; Mangolini, F.; Weber, R. T.; Fornasiero, P.; Murray, C. B. Nonaqueous synthesis of TiO_2 nanocrystals using TiF_4 to engineer morphology, oxygen vacancy concentration, and photocatalytic activity. *J. Am. Chem. Soc.* **2012**, *134*, 6751−6761.
(26) Selloni, A. Crystal growth: Anatase shows its reactive side. *Nat. Mater.* **2008**, *7*, 613−615.
(27) Roy, N.; Sohn, Y.; Pradhan, D. Synergy of low-energy {101} and high-energy {001} TiO_2 crystal facets for enhanced photocatalysis. *ACS Nano* **2013**, *7*, 2532−2540.
(28) Liu, C.; Han, X.; Xie, S.; Kuang, Q.; Wang, X.; Jin, M.; Xie, Z.; Zheng, L. Enhancing the photocatalytic activity of anatase TiO_2 by improving the specific facet-induced spontaneous separation of photogenerated electrons and holes. *Chem.—Asian J.* **2013**, *8*, 282−289.
(29) Li, R.; Zhang, F.; Wang, D.; Yang, J.; Li, M.; Zhu, J.; Zhou, X.; Han, H.; Li, C. Spatial separation of photogenerated electrons and holes among {010} and {110} crystal facets of $BiVO_4$. *Nat. Commun.* **2013**, *4*, 1432.
(30) Li, C.; Zhang, P.; Lv, R.; Lu, J.; Wang, T.; Wang, S.; Wang, H.; Gong, J. Selective deposition of Ag_3PO_4 on monoclinic $BiVO_4$(040) for highly efficient photocatalysis. *Small* **2013**, *9*, 3951−3956.
(31) Yu, J.; Qi, L.; Jaroniec, M. Hydrogen production by photocatalytic water splitting over Pt/TiO_2 nanosheets with exposed (001) facets. *J. Phys. Chem. C* **2010**, *114*, 13118−13125.
(32) Han, X.; Kuang, Q.; Jin, M.; Xie, Z.; Zheng, L. Synthesis of titania nanosheets with a high percentage of exposed (001) facets and related photocatalytic properties. *J. Am. Chem. Soc.* **2009**, *131*, 3152−3153.
(33) Yu, J.; Fan, J.; Lv, K. Anatase TiO_2 nanosheets with exposed (001) facets: improved photoelectric conversion efficiency in dye-sensitized solar cells. *Nanoscale* **2010**, *2*, 2144−2149.
(34) Xiang, Q.; Lv, K.; Yu, J. Pivotal role of fluorine in enhanced photocatalytic activity of anatase TiO2 nanosheets with dominant (001) facets for the photocatalytic degradation of acetone in air. *Appl. Catal., B* **2010**, *96*, 557−564.
(35) Tian, F.; Zhang, Y.; Zhang, J.; Pan, C. Raman spectroscopy: A new approach to measure the percentage of anatase TiO_2 exposed (001) facets. *J. Phys. Chem. C* **2012**, *116*, 7515−7519.
(36) Frens, G. Controlled nucleation for the regulation of the particle size in monodisperse gold suspensions. *Nature Phys. Sci.* **1973**, *241*, 20−22.
(37) Rosseler, O.; Shankar, M. V.; Karkmaz-Le Du, M.; Schmidlin, L.; Keller, N.; Keller, V. Solar light photocatalytic hydrogen production from water over Pt and Au/TiO_2(anatase/rutile) photocatalysts: Influence of noble metal and porogen promotion. *J. Catal.* **2010**, *269*, 179−190.
(38) Tsukamoto, D.; Shiraishi, Y.; Sugano, Y.; Ichikawa, S.; Tanaka, S.; Hirai, T. Gold nanoparticles located at the interface of anatase/rutile TiO_2 particles as active plasmonic photocatalysts for aerobic oxidation. *J. Am. Chem. Soc.* **2012**, *134*, 6309−6315.
(39) Grunwaldt, J. D.; Kiener, C.; Wögerbauer, C.; Baiker, A. Preparation of supported gold catalysts for low-temperature CO oxidation via "size-controlled" gold colloids. *J. Catal.* **1999**, *181*, 223−232.
(40) Menard, L. D.; Xu, F.; Nuzzo, R. G.; Yang, J. C. Preparation of TiO_2-supported Au nanoparticle catalysts from a Au_{13} cluster precursor: Ligand removal using ozone exposure versus a rapid thermal treatment. *J. Catal.* **2006**, *243*, 64−73.
(41) Comotti, M.; Li, W. C.; Spliethoff, B.; Schüth, F. Support effect in high activity gold catalysts for CO oxidation. *J. Am. Chem. Soc.* **2006**, *128*, 917−924.
(42) Yin, H.; Wang, C.; Zhu, H.; Overbury, S. H.; Sun, S.; Dai, S. Colloidal deposition synthesis of supported gold nanocatalysts based on $Au-Fe_3O_4$ dumbbell nanoparticles. *Chem. Commun.* **2008**, 4357−4359.
(43) Wen, L.; Fu, J. K.; Gu, P. Y.; Yao, B. X.; Lin, Z. H.; Zhou, J. Z. Monodispersed gold nanoparticles supported on γ-Al_2O_3 for enhancement of low-temperature catalytic oxidation of CO. *Appl. Catal., B* **2008**, *79*, 402−409.
(44) Lopez-Sanchez, J. A.; Dimitratos, N.; Hammond, C.; Brett, G. L.; Kesavan, L.; White, S.; Miedziak, P.; Tiruvalam, R.; Jenkins, R. L.; Carley, A. F.; Knight, D.; Kiely, C. J.; Hutchings, G. J. Facile removal of stabilizer-ligands from supported gold nanoparticles. *Nat. Chem.* **2011**, *3*, 551−556.